Wideband Microstrip to 3-D-Printed Air-Filled Waveguide Transition Using a Radiation Probe

Ilona Piekarz, Jakub Sorocki, *Member, IEEE*, Nicolò Delmonte, *Member, IEEE*, Lorenzo Silvestri, Stefania Marconi, Gianluca Alaimo, Ferdinando Auricchio, and Maurizio Bozzi, *Fellow, IEEE*

***Abstract*— In this letter, a novel wideband microstrip to additively fabricated waveguide transition is presented. The proposed design takes advantage of the flexibility of 3-D printing to realize a highly integrated transition from the microstrip line on a printed circuit board (PCB) to an air-filled waveguide using an additively manufactured radiating probe. The idea is experimentally verified by the realization of an exemplary transition working within the X-band at $f_0 = 10.5$ GHz. The measured performance of the back-to-back transition proves its usefulness and possibility of utilization in highly integrated PCB-waveguide circuits. A PolyJet printing technology with copper electroplating was used in combination with PCB on microwave grade laminate. A bandwidth of $f_H/f_L = 1.8$ was obtained with the impedance match better than 9.5 dB and in-band insertion loss per transition below 1.1 dB.**

***Index Terms*— Additive manufacturing, printed circuits, transition, waveguide and PCB integration, X-band.**

I. Introduction

TRANSITIONS from waveguide to microstrip are widely discussed in the literature since they allow the integration of waveguide structures with the majority of RF circuits designed by using the microstrip technique. There are two main configurations of the transitions i.e., longitudinal and vertical ones. Most of the longitudinal transitions require the insertion of the microstrip-line part into the waveguiding structure [1], [2], which limits their use and makes the PCB-waveguide integration more difficult. On the other hand, vertical transitions [3], [4] enforce the perpendicular orientation of the microstrip and waveguide, leading to integration limitations. Recently, an air-filled waveguide, integrated with the PCB by sharing the common metal plane, which on one side serves as a ground plane for the microstrip transmission line and on the other side as one of the walls of the waveguide, has been proposed [5] as an alternate to the above arrangements. Apart from low-cost manufacturing, low weight, and high compactness, a great advantage of such realization is the ease of integration of low-loss passive waveguide/microstrip and active microstrip components. Thus, the development of a compatible transition from one guiding structure to another is of great importance.

In this letter, we propose a wideband microstrip-to-waveguide transition that exploits to a great extent the 3-D-printing fabrication with selective metal deposition and exceeds the bandwidth capability of one in [5]. To launch the EM wave into the waveguide, a radiation probe, protruding from the microstrip line, is introduced at an offset from the shorted end of the waveguide and the open end of the microstrip line. Moreover, the probe is proposed to be embedded in a U-shaped waveguide part that is 3-D printed and selectively metalized to leave a nonconducting gap from the bottom wall. The radiating probe feeding was proven to provide a broadband response in an all-metal waveguide to coaxial transitions, and thus, similar benefits are expected here. Such compact transition complements the benefits of the integrated low-loss waveguide realization. The presented approach was experimentally verified at X-band by measurements of a fabricated exemplary transition in back-to-back configuration confirming its usefulness.

II. Microstrip-to-Waveguide Transition Using a Radiation Probe

A general drawing of the proposed microstrip-to-waveguide transition is shown in Fig. 1. Its construction is derived from a right-angle E-plane coaxial line to waveguide transition. The transition is composed of a printed circuit board (PCB) with at least two layers of metallization, hosting the microstrip line, and a metal-coated plastic 3-D component, hosting the waveguide. The ground plane of the microstrip line on the bottom part of the laminate serves at the same time as the top metal wall of the waveguide. The transition from one guiding structure to another is realized through a radiating probe that is an integral part of the plastic 3-D component with partial metallization on its upper half (h_1). The probe is in direct (galvanic) contact with the microstrip line. Two contact planes can be used for a more reliable connection, i.e., a horizontal one at a via-connected pad (d_2) with isolation ring (d_3) located on the ground plane side and a vertical one at via wall the hole (d_1) of which it accepts a corresponding size probe extension. Moreover, the microstrip

Manuscript received 28 January 2022; revised 28 March 2022 and 19 April 2022; accepted 4 May 2022. Date of publication 19 May 2022; date of current version 7 October 2022. This work was supported by the National Science Centre, Poland under Grant 2019/34/E/ST7/00342. The work of Jakub Sorocki was supported by the Polish National Agency for Academic Exchange (NAWA) through the Bekker Program under Grant PPN/BEK/2019/1/00240. *(Corresponding author: Ilona Piekarz.)*

Ilona Piekarz and Jakub Sorocki are with the Institute of Electronics, AGH University of Science and Technology, 30-059 Kraków, Poland, and also with the Department of Electrical, Computer and Biomedical Engineering, University of Pavia, 27100 Pavia, Italy (e-mail: ilona.piekarz@agh.edu.pl).

Nicolò Delmonte, Lorenzo Silvestri, and Maurizio Bozzi are with the Department of Electrical, Computer and Biomedical Engineering, University of Pavia, 27100 Pavia, Italy.

Stefania Marconi, Gianluca Alaimo, and Ferdinando Auricchio are with the Department of Civil Engineering and Architecture, University of Pavia, 27100 Pavia, Italy.

Color versions of one or more figures in this letter are available at https://doi.org/10.1109/LMWC.2022.3173407.

Digital Object Identifier 10.1109/LMWC.2022.3173407

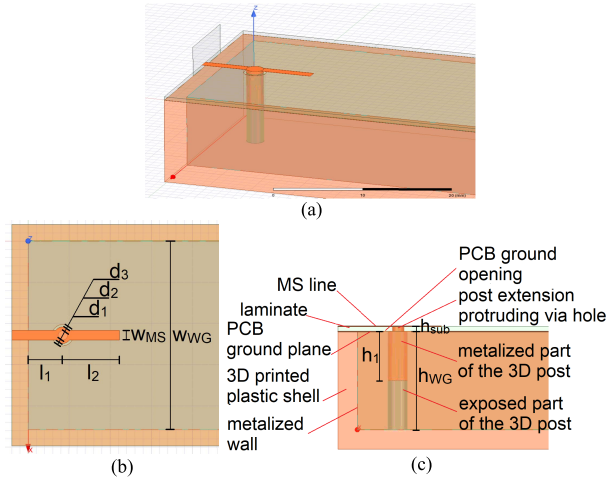

Fig. 1. (a) Three-dimensional view, (b) top view, and (c) side view of the proposed microstrip-to-waveguide transition along with marked parameters.

line is loaded at one end with an open-ended stub, which is necessary for impedance matching, while the waveguide is loaded with a short, both at a given offset from the probe. The microstrip linewidth w_{MS} is selected in a way to ensure a given characteristic impedance (here 50 Ω) considering the dielectric stratification. Offset lengths l_1 from the waveguide end short and l_2 from the microstrip end open along with the radiation probe length h_1(metalized part of the post) affect the transition's center frequency and bandwidth. It is worth noting that depending on the waveguide cross section, the wave impedance varies and so does the electric field distribution for which the probe is being tuned. Initial values for l_1 and h_1 can be calculated using the rule-of-thumb formulas for right-angle waveguide-to-coax transitions with extrapolation onto l_2. In such a case, the distances from the waveguide back-short to the probe and from the probe to the microstrip open are assumed to be equal $l_1 = l_2 = \lambda/4$ @ f_0, whereas for the probe length, $h_1 = 3/16\ \lambda$ @ f_0. The probe diameter d_2 minimal size must ensure the mechanical integrity of the printed post. Notably, an opening in the waveguide's wall is present where the printed post attaches to the shell, which when too large may introduce additional radiation losses. Moreover, the radiation probe is established on a dielectric post the presence of which it affects the E-field distribution. For a lossy material, this might be a source of additional dielectric loss, especially when considering increased E-field concentration in this area. To mitigate the above, the metalized part of the post might be kept at a minimum diameter or enlarged, while the nonmetalized support kept at a minimum diameter to reduce losses. In the next step, l_1 and h_1 are to be fine-tuned together with l_2 and, if necessary, with d_2 to optimize impedance matching and bandwidth of the transition.

A hybrid fabrication is intended for the proposed transition and by extension, circuits integrating it, i.e., the waveguide part can be manufactured in a two-step process: 3-D printing out of plastic, followed by selective metallization (masking and peel-off technique can be used as in, e.g., [6] and [7] to obtain metal probe of a given penetration depth into the cross section of the waveguide).

TABLE I

DIMENSIONS FOR AN EXEMPLARY MICROSTRIP-TO-WAVEGUIDE TRANSITION USING A RADIATION PROBE OPERATING IN THE X-BAND

Variable	Value (mm)	Variable	Value (mm)
w_{MS}	1.16	h_{sub}	0.51
d_1	2.00	l_1	6.70
d_2	2.00	l_2	7.40
d_3	2.60	h_1	4.87
w_{wg}	22.86	h_{wg}	10.16

III. EXPERIMENTAL RESULTS

To validate the proposed concept, an exemplary transition was designed to operate within X-band at the center frequency $f_0 = 10.5$ GHz. A standard WR-90-sized waveguide geometry was used. The waveguide was integrated through its broad wall with a double-sided PCB on a 20-mil-thick Taconic RF-35 laminate ($Dk = 3.5$ and $\tan\delta = 0.0017$). The radiating probe diameter d_2 was chosen as a tradeoff between sufficient mechanical stiffness and ease of mating with a 50-Ω line of width w_{MS}. Moreover, slot diameter d_3 in the PCB's ground plane was chosen as a tradeoff between minimizing radiation outside the waveguide and fabrication tolerances to avoid shortening the probe to the ground. Having fixed the above, one needs to find lengths l_1, l_2, and h_1. For the sake of this design, a numerical optimization using a full-wave EM model was applied to obtain an impedance match better than 10 dB for the entire waveguide's TE10 mode optimal bandwidth (8.2–12.4 GHz). The circuit was simulated in the microstrip-to-waveguide configuration using *Ansys HFSS* software and the results are shown in Fig. 2, while the final transition geometry is listed in Table I. The upper resonance can be attributed to the waveguide back-short, while the lower one can be attributed to the microstrip open stub. The transition operates within 7.8–12.9 GHz ($f_H/f_L \approx 1.65$) with an average insertion loss of 0.18 dB per transition (bulk copper waveguide wall, no contact resistance between waveguide and PCB metals, lossless post dielectric, and lossy laminate). The lossy dielectric of the radiation probe's post adds an extra ∼0.04 dB of loss, while opening in the bottom waveguide wall has a neglectable impact.

The manufacturing process requires the fabrication of two parts that are assembled afterward, namely, PCB and 3-D shell. The PCB was fabricated using the LPKF ProtoMat E33 CNC milling machine. On the other hand, for the fabrication of the U-shaped waveguide part with radiation probe, additive manufacturing was employed by combining 3-D printing in polyjet technology using high-resolution Stratasys Objet 260 Connex 3 machine out of FullCure Vero White resin (estimated $Dk \approx 2.8$ and $\tan\delta \approx 0.01$) followed by selective copper coating. The model was oriented for 3-D printing so that no support material would touch the three internal walls of the waveguide, ensuring a smooth surface leading to lower conductor losses. After that, to mask the part of the probe that is not to be coated, a precut Kapton tape was temporarily attached before metallization. The electroplating process was used after coating the parts with conductive paint, to grow roughly a 5-μm-thick copper layer.

An important aspect of the integrated microstrip-waveguide assembly, apart from the elements' alignment and mechanical

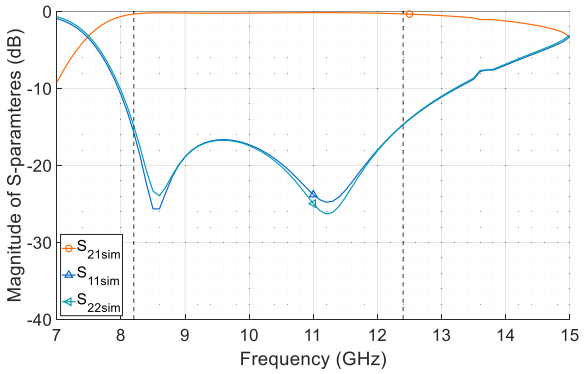

Fig. 2. EM simulated *S*-parameters of the designed transition operating in the X-band. Port #1 is the microstrip side, while Port #2 is the waveguide side.

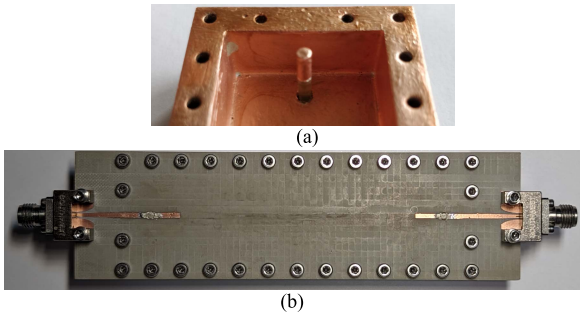

Fig. 3. Photographs of the fabricated X-band microstrip-to-waveguide transition in the back-to-back configuration: (a) copper-printed waveguide with radiating probe and (b) full assembled stack up with PCB's top view.

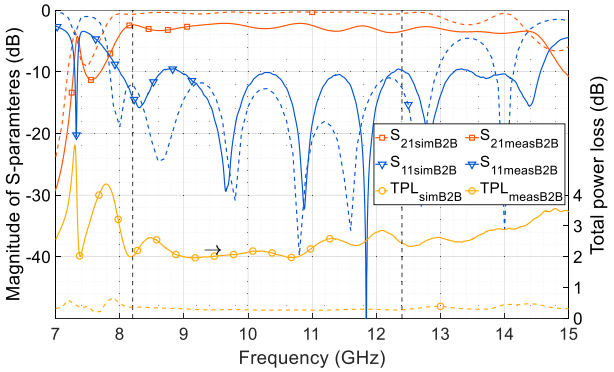

Fig. 4. *S*-parameters of the demonstrator in back-to-back: measured (solid lines) versus EM data (dashed lines) with TPL overlaid. TPL includes the coax-to-MS launchers loss.

integrity, is to ensure low-resistance contact between PCB's ground plane and metalized waveguide top flanges. To mitigate this issue and reduce the number of factors affecting the transition's performance, screws were used to clamp the assembly using dedicated through-holes. Moreover, a low-resistance contact is required in the region where a via-pad on the microstrip line connects to the metalized part of the plastic post effectively exciting the probe. This can be ensured by press-fitting the post extension or adding extra solder of conductive adhesive.

Photographs of the manufactured exemplary X-band transition in the back-to-back configuration are shown in Fig. 3, whereas the measurement results are shown in Fig. 4. The circuit was measured using the Agilent PNA N5224A Vector Network Analyzer at 10-MHz steps interfaced using 2.92-mm southwest end-launch connectors at which the reference plane was set. The fabricated transition performance is close to what was expected from the simulation. The transition operates from 8 to 14.5 GHz ($f_H/f_L \approx 1.8$). A reduction to 9.5 dB or below of impedance matching and a slight shift upward of the response is visible. The performance drop, compared to EM simulation (model assumptions as for a single transition), can be mostly attributed to finite fabrication and assembly tolerances as well as metallization and contact quality between the parallel metallic surfaces. In particular, the former affects the region where the metal-coated plastic probe contacts the via-pad on the PCB. The latter is important since the seam is in the waveguide's region of higher current concentration. The in-band total power loss (TPL $= 1 - |S_{21}|^2 - |S_{11}|^2$) at center frequency is below 1.1 dB per transition. Within the per transition loss, it is estimated that ∼0.4 dB of loss is due to the coax-to-MS launcher. The total waveguide length between end shorts within the demonstrator is 85 mm (estimated loss of ∼0.1 dB/cm [5]).

Finally, the proposed transition was compared with other solutions presented in the literature with a summary shown in Table II. As seen, the proposed transition not only features parallel orientation of the two guiding structures but also the widest bandwidth, not to mention the integration aspect and low-cost realization due to the utilization of AM process. As a field for improvement, the effective resistance of the 3-D printed component metallization along with contact resistance between parts is seen as those that affect the in-band insertion losses.

TABLE II

SUMMARY OF THE PROPERTIES AND PERFORMANCE OF VARIOUS STATE-OF-THE-ART MICROSTRIP-TO WAVEGUIDE TRANSITIONS

	PCB vs WG	Feed vs. WG	Vias	Loss per transiton#	BW* f_h/f_l	WG fabric. proc.	WG
[8]	Separate	Parallel	yes	< 1 dB	>1.5	Metal milling	WR-90
[9]	Separate	Inline	no	< 1 dB	1.1	Metal milling	WR-12
[10]	Separate	Perpend.	yes	< 1.4 dB	1.2	Metal milling	WR-28
[2]	Separate	Inline	no	< 0.9 dB	1.5	Metal milling	WR-90
[5]	Integrated	Parallel	no	1.5 dB avg.	1.4	Coated 3D printed	WR-90
[11]	Separate	Inline	no	< 0.4 dB	1.5	Metal milling	WR-10
[12]	Separate	Perpend.	no	< 1 dB	1.5	Metal milling	WR-90
This	Integrated	Parallel	yes	< 1.1 dB	1.8	Coated 3D printed	WR-90

*$|S_{11}| \leq$ -10 dB; # feeding line length varies among designs

IV. CONCLUSION

A novel parallel microstrip-to-waveguide transition that exploits to a great extent the 3-D-printing fabrication with selective metal deposition was presented in this letter. To launch the EM wave into the waveguide, a radiation probe is employed. The probe is proposed to be embedded in a U-shaped waveguide part that is 3-D printed and selectively metalized. As a result, broadband and compact transition are obtained. The presented approach was experimentally verified at the X-band showing the advantages of the solution and identifying ways to improve the performance.

REFERENCES

[1] H.-W. Yao, A. Abdelmonem, J.-F. Liang, and K. A. Zaki, "Analysis and design of microstrip-to-waveguide transitions," *IEEE Trans. Microw. Theory Tech.*, vol. 42, no. 12, pp. 2371–2379, Dec. 1994.

[2] N. Kaneda, Y. Qian, and T. Itoh, "A broad-band microstrip-to-waveguide transition using quasi-yagi antenna," *IEEE Trans. Microw. Theory Techn.*, vol. 47, no. 12, pp. 2562–2567, Dec. 1999.

[3] Y. Li and K.-M. Luk, "A broadband V-band rectangular waveguide to substrate integrated waveguide transition," *IEEE Microw. Wireless Compon. Lett.*, vol. 24, no. 9, pp. 590–592, Sep. 2014.

[4] N. T. Tuan, K. Sakakibara, and N. Kikuma, "Bandwidth extension of planar microstrip-to-waveguide transition by controlling transmission modes through via-hole positioning in millimeter-wave band," *IEEE Access*, vol. 7, pp. 161385–161393, 2019.

[5] J. Sorocki *et al.*, "Additively fabricated air-filled waveguide integrated with printed circuit board using a through-patch transition," *IEEE Microw. Wireless Compon. Lett.*, vol. 31, no. 11, pp. 1207–1210, Nov. 2021.

[6] J. A. Byford, M. I. M. Ghazali, S. Karuppuswami, B. L. Wright, and P. Chahal, "Demonstration of RF and microwave passive circuits through 3-D printing and selective metalization," *IEEE Trans. Compon., Packag., Manuf. Technol.*, vol. 7, no. 3, pp. 463–471, Mar. 2017.

[7] J. Sorocki, I. Piekarz, S. Gruszczynski, K. Wincza, and J. Papapolymerou, "Application of additive manufacturing technologies for realization of multilayer microstrip directional filter," in *Proc. IEEE 68th Electron. Compon. Technol. Conf. (ECTC)*, San Diego, CA, USA, May 2018, pp. 2382–2388.

[8] M. Gholami and M. N. Jazi, "Implementation of a low loss microstrip to waveguide transition in X-band using CAD methods," *J. Electromagn. Waves Appl.*, vol. 23, nos. 8–9, pp. 1133–1141, 2009.

[9] B. Boukari, E. Moldovan, S. Affes, K. Wu, R. G. Bosisio, and S. O. Tatu, "Robust microstrip-to-waveguide transitions for millimeter-wave radar sensor applications," *IEEE Antennas Wireless Propag. Lett.*, vol. 8, pp. 759–762, 2009.

[10] A. Mozharovskiy, S. Churkin, A. Arternenko, and R. Maslcnnikov, "Wideband probe-type waveguide-to-microstrip transition for 28 GHz applications," in *Proc. 48th Eur. Microw. Conf. (EuMC)*, Sep. 2018, pp. 113–116.

[11] C. Wu *et al.*, "Millimeter-wave waveguide-to-microstrip inline transition using a wedge-waveguide iris," *IEEE Trans. Microw. Theory Techn.*, vol. 70, no. 2, pp. 1087–1096, Feb. 2022.

[12] Y.-C. Lee, J.-C. Guo, and C.-L. Wang, "Compact and broadband microstrip line-to-rectangular waveguide transition using magnetic coupling resonator and ground resonators," *IEEE Trans. Microw. Theory Techn.*, vol. 69, no. 12, pp. 5300–5304, Dec. 2021.